APPLICATION OF BARCELONA TEST FOR CONTROLLING ENERGY ABSORPTION CAPACITY OF FRS IN UNDERGROUND MINING WORKS

SERGIO CARMONA[1]

Departamento de Obras Civiles, Universidad Técnica Federico Santa María

Valparaíso, Chile.

CLIMENT MOLINS

Departamento de Ingeniería Civil y Ambiental

Universitat Politècnica de Catalunya, Barcelona Tech

Barcelona, España

SERGIO GARCÍA

Vicepresidencia CODELCO – Chile

ABSTRACT

In recent years in Chile, the use of fiber reinforced shotcrete (FRS) has been widely extended in underground works, particularly in tunnels for roads, mines and hydroelectric projects. In these projects, the design of the supports is mainly based on the modified Q–Barton method, which relates the rock mass quality to the minimum energy absorption capacity of the FRS, which is determined by the square panel test, with panels filled during spraying. However, to obtain these specimens, complex procedures must be followed both on-site and, in the laboratory, and the results obtained present a large scatter.

To improve the execution control of the FRS lining of tunnels, an empirical correlation has been developed between the square panel test of a synthetic-fiber reinforced concrete and the double-punch Barcelona test of cylinders, at laboratory level.

[1]Corresponding author: sergio.carmona@usm.cl, Casilla 110- V Valparaíso, Chile. Tel. +56322654382 Fax +56322654115

The application of such a correlation to a concrete sprayed on-site using the same fiber has proven satisfactory, with a difference between the experimental and the correlated measurement of 2.6%. Then, the methodology presented in this paper can be applied to control the FRS to any other case.

KEYWORDS: squared panel test, energy absorption capacity, fiber reinforced shotcrete, tunneling, BCN test.

1. INTRODUCTION

In recent years in Chile, the use of shotcrete and fiber reinforced shotcrete (FRS) has been widely extended in underground works, particularly in tunnels for roads, mining and hydroelectric projects, as shown in Figure 1. In these projects, the design of the supports is mainly based on the modified Q-Barton method (Barton *et al*., 1974; Barton and Bandis, 1990), which relates the quality of the rock mass to the minimum energy absorption capacity of the FRS, which is determined using a square panel test with panels filled during spraying, following the recommendations provided in the "European Specification for Sprayed Concrete" published in 1996 by the European Federation of National Associations Representing Producers and Applicators of Specialist Building Products for Concrete (EFNARC,1996) or according to the EN 14488–5:2006 standard (CEN, 2006).

Figure 1. FRS spraying in mining work in Chile.

However, these tests require large and heavy specimen samples, which must be filled while spraying FRS onto the tunnel lining. This often causes the panels to present defects or damage that alter the results and increase their scatter, with coefficients of variation (CoV) above 15% and sometimes above 20% between specimens of the same sample (Carmona and Molins, 2017).

On the other hand, the double-punch test (DPT) or Barcelona test (BCN test) proposed by Molins *et al*. (2006; 2009) has proven to be adequate for the control of fiber reinforced concrete (FRC) in construction and has been standardized in Spain by AENOR as UNE 83515 (AENOR, 2010). This test has several advantages with respect to other standard procedures for characterizing FRC toughness, among which is the use of relatively small samples with large fracture surfaces, which can be cores drilled from the hardened concrete as presented in Aire *et al*. (2015) and can be tested using conventional testing machines. This test also presents lower scatter than the common three-point and four-point bending tests (Carmona *et al*., 2018).

The main objective of this paper is to present a direct correlation between the energy absorption capacity determined by the square panel test and the BCN test, with the aim of substituting the square panel test by the BCN test as a control test in tunnel works with FRS linings. To this end, the results of three extensive experimental investigations are presented: one developed on samples made in the laboratory and the other two on samples and cores produced in different tunnel works. The laboratory investigation allowed proposing a correlation between the energy absorbed by the two tests, whereas the two on-site investigations allowed the validation of the proposed correlation.

This paper is the third of a trilogy, in which the BCN test has been experimentally correlated with the bending tests given in standards EN – 14651 (Carmona *et al*., 2018)

and ASTM C 1609 (Carmona and Molins, 2019), widely used for the characterization of fiber reinforced concretes.

2. ENERGY ABSORPTION CAPACITY OF THE FRS

According to the EN 14488–1 standard (CEN, 2005a) and the recommendation of EFNARC (1996) for hand spraying, the minimum plan dimensions of the samples obtained on-site must be 500 × 500 mm and 600 × 600 mm, respectively. For robotic spraying, both standards establish a minimum dimension of 1000 × 1000 mm for panel. The energy absorption capacity is determined by testing square panels of 600 × 600 mm and 100 mm in thickness, which is supported by a rigid steel frame at their four edges, leaving a span of 500 mm between opposite edges. The test is performed under actuator displacement control at a central deflection rate of 1.0 mm/min in the case of the EN 14488–5 standard and of 1.5 mm/min according to the EFNARC recommendation. The load is applied at the center of the panel over a contact surface of 100 × 100 mm, as shown in Figure 2.

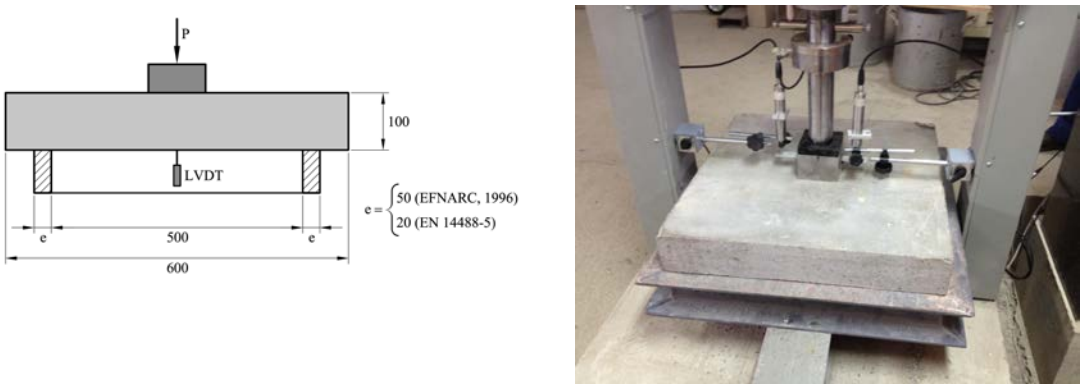

Figure 2. Set up given for square panel.

During the test, the load and central deflection are continuously recorded until a central deflection of at least 30 mm is achieved. Using that response, the energy absorption capacity, up to a central net deflection δ = 25 mm (E_{25}), is calculated as:

$$E_{25} = \int_0^{25} P(\delta) \cdot d\delta \quad (1)$$

where $P(\delta)$ is the load as a function of deflectionδ.

The results of square panel tests present high variability, with intra-sample coefficients of variation (CoV) that can exceed 20%. This is due to multiple typical factors of the spraying process such as pressure, distance, and spraying angle as well as sampling, including the support conditions of the mold, curing, transport and subsequent cutting of the panels in the laboratory. In addition to the above, the panels are heavy and difficult to handle, both on-site as well as in the laboratory, which causes many panels to present damage or defects that alter the results.

Another source of error is the deflection measuring point. The load-deflection curves obtained by measuring the deflection on the upper and lower faces of a panel are shown in Figure 3a. It can be observed that for a central defection of 25 mm, as measured on the lower face of the panel, the deflection measured on the upper face is significantly lower, with a consequent effect on the calculation of the absorbed energy.

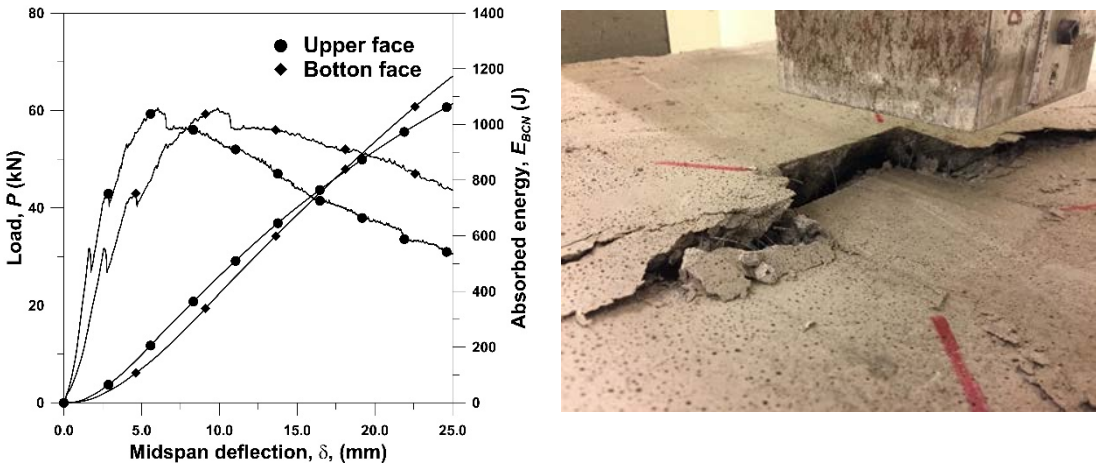

Figure 3. (a) Comparison of the measurement of the central deflection with respect to the lower and upper face of the panel; (b) Final state of the top face of an FRS panel after the test.

A punching failure caused by the load on the upper face of the panel, as observed in the concretes reinforced with medium and high fiber contents, is shown in Figure 3b. This failure causes that the loading platen penetrates the upper face of panel, which decreases

the displacement measured on that face with respect to the central deflection recorded on the lower face of the panel.

3. DISSIPATED ENERGY IN BCN TEST

As Barcelona (BCN) test is known an indirect tension test proposed by Molins *et al*. (2009) to determine fiber reinforced concrete properties (ACI, 2016). In this test, a cylindrical specimen of FRC is subjected to a double punching compression load by means of two cylindrical steel punches placed at the center of the upper and the lower faces, respectively, as shown in Figure 4a.

Figure 4. (a) BCN test setup; (b) Typical final state of specimens subjected to double punching tests.

According to the UNE 83515 standard (AENOR, 2010), the cylindrical specimen dimensions are $d = h = 150$ mm, i.e., $h/d = 1$, and the steel wedges diameter is $a = d/4$. In contrast to other indirect tensile tests used for controlling the FRC properties, this test can be performed in a conventional testing system under stroke displacement control at a rate of 0.5 ± 0.05 mm/min. During the test, the applied load and the circumferential deformation measured at half the height of the specimen must be continuously recorded. On the specimen, the applied load produces a conical volume under triaxial compression stress beneath the punches, increasing the cylinder diameter and producing tensile stresses perpendicular to the radial planes of specimen. Due to this tensile stress with cylindrical

symmetry, when the stress exceeds the tensile strength of concrete, cracks perpendicular to the field propagate through the specimen. This allows that the compression cones penetrate the cylinder increasing the specimen radius and producing two or more cracks. Then, the final state of the specimen presents two aligned cracks, or three cracks arranged approximately at 120° or, sometimes, four perpendicular cracks as can be seen in Figure 4b (Carmona *et al*., 2012).

When the specimen cracks, the circumferential dilatation corresponds to the total circumferential opening displacement ($TCOD$) and the energy dissipated can be calculated as:

$$E_{BCN,x} = \int_0^{Rx} P(Rx) \cdot d(Rx) \quad (2)$$

where $E_{BCN,x}$ is the energy dissipated at a certain value of total circumferential deformation R_x. According to the standard UNE 83515, the energy should be determined at $R_x = 2.0$ mm, 2.5 mm, 4.0 mm, and 6.0 mm.

Due to its simplicity and greater knowledge of the response of the FRC subjected to the BCN test, supported by a large number of experimental researches (Carmona *et al*., 2012; 2013; Aire *et al*., 2015), numerical (Pros *et al*., 2011; 2012; Pujadas *et al*., 2013) and experimental correlations with the bending tests given in the standards EN - 14651 (Carmona *et al*., 2018) and ASTM C 1609 (Carmona and Molins , 2019), this test has begun to be used to evaluate the post-cracking behavior of FRC, as can be seen in the research performed by Chao *et al*., 2012; Pujadas *et al*., 2014; Kim *et al*., 2015; Carmona *et al*., 2016; Choumanidis *et al*., 2017; Rambo *et al*., 2018, and has been proposed as a control test for fiber-reinforced shotcrete in some large tunnel projects, such as the Metro de Lima (Geocontrol, 2015) and Chuquicamata Underground (*Chuquicamata Subterránea*) Project of CODELCO – Chile (Carmona, 2017).

4. EQUIVALENCE BETWEEN PANEL TEST AND DPT

In the last years, different correlations among bending tests and BCN test had been proposed by Conforti *et al*. (2017), Carmona *et al*. (2018; 2019) based on crack opening (w). Then, an equivalence between the square panel test and the BCN test should be proposed in terms of w; therefore, it is necessary to establish a relationship between the midspan net deflection, δ, recorded in the panel test and the crack opening displacement (COD) in the panel, w_{PANEL}.

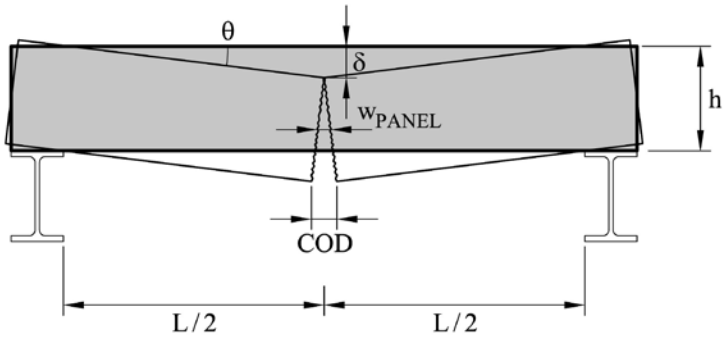

Figure 5. Geometric relationship on cracked square panel.

For a square panel with a central crack, as shown Figure 5, considering geometric relationships and that w_{PANEL} corresponds to half of the COD on the surface of the lower face of the panel, the following relation can be established:

$$w_{\mathrm{PANEL}} = \frac{COD}{2} = \frac{2 \cdot \delta \cdot h}{l} \tag{3}$$

In the case the standardized square panel, with $h = 100$ mm, and $l = 500$ mm, Eq. (3) yields $w_{PANEL} = 0.4\ \delta$.

On the other hand, assuming three radial cracks in the failure mechanism of the FRC cylinder subjected to a DPT, which opens increasing the diameter, $\Delta\phi$, the average crack opening, w_{BCN}, can be estimated with the following expression (Molins *et al*., 2009):

$$w_{\mathrm{BCN}} = \frac{TCOD}{3} \tag{4}$$

Then, equating Equations (3) and (4), the following relationship can be proposed:

$$w_{\mathrm{PANEL}} = \frac{COD}{2} = \frac{2 \cdot \delta \cdot h}{l} = w_{\mathrm{BCN}} = \frac{TCOD}{3} \tag{5}$$

This equation relates the mean crack opening with the crack opening displacement and the deflection measured in the square panel test with the total crack opening displacement of cylinders in the BCN test. Therefore, it allows establishing equivalence between both tests based on similar crack opening.

Using equation (5), the crack opening equivalent to a $TCOD = 6$ mm corresponds to a net deflection of the panel (δ) of 5 mm. However, there is a low plastic deformation of the FRC at that deflection of the panel, as can be seen in the curves obtained by Carmona and Molins (2017). This is because the net deflection in the square panel test includes: (1) the adaptation of the panel to the support on the frame and (2) the elastic flexural deformation of the panel, which are about two or more millimeters, as can be seen in the Figure 3a.

In addition, according to the EFNARC recommendation and the EN 14488–5 standard, the energy absorption capacity of the FRS should be determined at a net midspan deflection $\delta = 25$ mm, which represents an advanced cracking and damage state of the panel with a high plastic deformation. Then, to establish an experimental correlation with the BCN test, it has been proposed to compare E_{25} with $E_{BCN,6}$, defined here as the energy dissipated by the cylinder subjected to a DPT at a $TCOD$ = 6 mm, which in the BCN test is also equivalent to an advanced crack opening state, as can be seen in Fig. 4b. To develop this proposed correlation, three values of E_{25} and $E_{BCN,6}$ corresponding to three different fibers content were determined experimentally.

5. EXPERIMENTAL DETAILS

To establish the proposed experimental correlation between both tests, the following research was undertaken.

5.1. Design of experimental research

The research at laboratory level was designed taking in account the following criteria based on Chilean tunnel lining construction practice. The concrete matrix was designed by a supplier of FRS for tunneling works. In fact, it was a concrete mix used in a real tunneling work where fiber BC – 54 was used. This type of fibers is widely used in FRS for tunneling in Chile with a fiber contents commonly between 4 kg/m^3 and 5.5 kg/m^3. Then, contents of 4 kg/m^3, 8 kg/m^3 and 12 kg/m^3 were selected to establish the correlation. Although the last fiber content can be seen as very high, it was chosen to evaluate a possible saturation effect of fibers in the tension response of FRS when contents are high. The minimum number of specimens tested *per* determination was fixed in nine because this is the amount necessary to produce a determination with a probability of 95% of determining differences of 10% in the mean with a 90% of significance, assuming that the distribution is normal and the coefficient of variation is 5% (Kuehl, 2001).

5.2. Materials

The concretes were prepared with a Portland pozzolanic cement of Type IP (ASTM, 2018) and crushed river sand; the mix dosage is presented in Table 1, and fibers features are given in Table 2.

Table 1. Features and properties of tested FRS.

Material (kg/m^3)		Concrete		
		FRS – 4	FRS – 8	FRS – 12
Cement type IP		420		
Sand 0/10		1655		
Superplastizicer admixture		2.10		
Superfluidifying admixture		2.10		
Active admixture		2.94		
Water		215		
Fiber content		4	8	12
Number of specimens	BCN test	10	9	10
	Square panel test	10	10	10

	Compressive test	3	3	3
Concrete properties				
Compressive strength, f_c (MPa)		39.5	40.9	42.3
V_f (%)		0.44	0.88	1.32

Table 2. Synthetic fiber properties (manufacturer's data).

Designation	l_f (mm)	d_f (mm)	λ_f l_f/d_f	f_{st} (MPa)	E (GPa)	Fibers/kg N°
BC – 54	54	0.84*	64.3	640	12	37000

(*) Equivalent diameter determined with the manufacturer's information.

The concretes were prepared at the laboratory using a conventional paddle mixer of 200 liters' capacity. For the BCN test, the specimens were cast in cylindrical molds with a diameter of 150 mm and a height of 150 mm. The panels were cast in steel molds of 600 × 600 × 100 mm. The quantity of specimens for each concrete are given in Table 1. All specimens were demolded after 24 hours and kept in a fog room, until testing. Table 1 also includes the results of the compression tests.

5.3. Tests and results

The panel tests were conducted in a hydraulic closed-loop control system of 100 kN capacity, under deformation control. The deflection was measured with a LVDT of 50 mm range, placed in the center bottom face of the specimen. The load and the deflection were recorded continuously by the testing system at a rate of 3 data/s. The mean curves obtained with each tested concrete are shown in Figure 6.

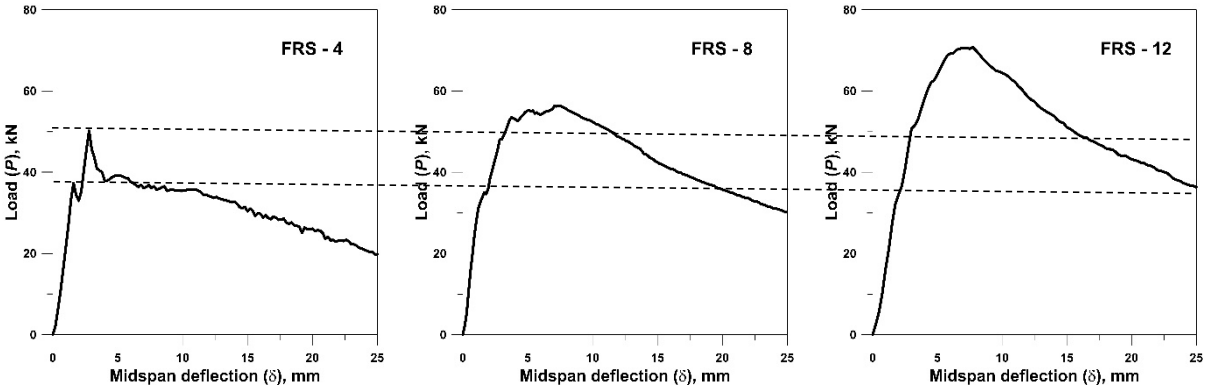

Figure 6. Mean $P - \delta$ curves obtained with panel tests.

(a) (b)

(c) (d)

Figure 7. (a) Crack pattern of FRS-4 panels after the test; (b) Rotation between portions of the panels of the FRS–4 series; (c) Evidence of the friction of the panel on the support framework; (d) Punching shear failure observed in panels with medium and high fiber amounts.

In the FRS–4 curve, a first peak was observed at an average load of 37.3 kN, with a central deflection δ = 1.60 mm associated with the formation of the first crack, and a second peak at an average load of 50.2 kN and δ = 2.80 mm when the second crack was produced. In these concretes, the cracks were usually oriented in the form of an × or +, as shown in Figure 7a. After the second peak, a softening was observed, with a gradual decrease in the load sustained by the FRS, which reached an average load of 19.8 kN at a central deflection of 25 mm. For advanced deflection levels (see Figure 7b), a high rotation of the portions of the cracked panel can be observed, with friction between the supporting edge and the edges of the panel, as shown in Figure 7c.

In the FRS–8, the first crack was obtained at an average load of 34.5 kN and δ = 1.77 mm, and the second crack was produced at a load P = 47.8 kN and δ = 3.06 mm. Subsequently, the load continued to increase, with local peaks associated with the formation of other cracks, until a maximum absolute load P = 56.5 kN was reached at δ = 7.03 mm. A softening was then observed whereby the load gradually decreased, reaching a load P = 30.0 kN at a deflection δ = 25 mm.

As can be observed in Figure 6, the loads corresponding to the first and second cracks do not seem to depend on the amount of reinforcing fiber. However, in the panels reinforced with medium and high amounts (FRS–8 and FRS–12, respectively), a flexural crack was initially produced, which caused the first peaks that can be observed in the $P - \delta$ curves. However, due to the higher amount of fibers present, the testing system had to increase the applied load to maintain the established deformation rate, which in addition to the friction force developed in the supported section of the panel gave rise to a punching

failure, which is reflected in the formation of cracks around the loaded section, as can be observed in Figure 7d, limiting the work of the fibers in tension and distorting the measurement of the deflection performed on the upper face of the panel.

To explain the failure mechanism of the FRS square panel, the theoretically maximum load that must be reached in the test was determined based on a plastic analysis of the behavior of a slab subjected to loading. How such loads are evaluated considering the plastic bending mechanism plus the arch effect introduced by the friction of the panel with the support frame is shown in Appendix 1. It was observed that for the panels with 4 kg/m^3 of fiber, such a load is very close to the load resisted in the test. However, for the panels with 8 and 12 kg/m^3 of fiber, the estimated loads that must be resisted were 68% and 88% higher than the experiment, respectively. The higher bending capacity of the FRS, the greater the difference from the results of the square panel. This shows that there is another ultimate mechanism that limits the loading capacity of the panels. It is, without a doubt, a mechanism associated with punching.

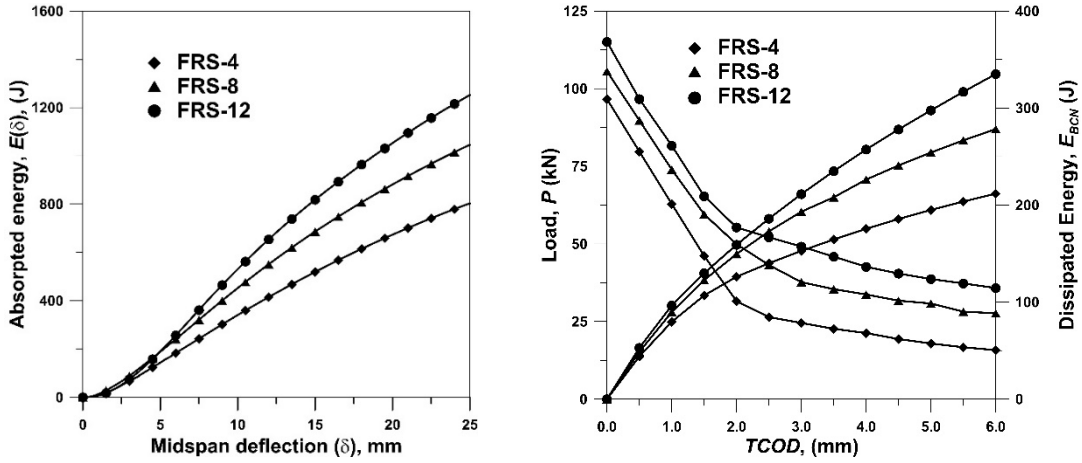

Figure 8. (a) Average $\delta - E_{25}$ curves obtained testing squared panel of each concrete studied; (b) Mean $P - TCOD$ and $E_{BCN} - TCOD$ responses obtained with BCN tests of each tested concrete.

The energy absorption capacity of each FRS was calculated using equation (1), obtaining the curves presented in Figure 8a. Considering that an FRS energy absorption capacity of 1000 J is specified in most projects, it is observed that this capacity is reached in the laboratory with 8 kg/m^3 of fiber.

On the other hand, the BCN tests were carried out using a conventional hydraulic system of 3 MN capacity controlled by stroke displacement at a constant rate of 0.5 mm/min. Following the standard UNE 83515, the circumferential dilatation was measured by means of an extensometer of 12 mm range, fixed to the ends of a chain and placed at half the height of the specimen. The test data were recorded by a data acquisition system at a frequency of two data per second. Figure 8b shows the mean $P - TCOD$ curves recorded during the BCN tests. In all these curves the $TCOD$ is close to zero until the maximum load is reached and, then, increases when cracking of specimen occurs. In the post – cracking regime the material exhibits a softening, governed by the fiber content.

The dissipated energy by the FRS during the cracking process was calculated using equation (2), obtaining the $E_{BCN} - TCOD$ curves which are also presented in Figure 8b.

6. EXPERIMENTAL CORRELATION BETWEEN TESTS

According to equation (5), the total crack opening of $TCOD = 6$ mm corresponds to a net deflection of the panel of $\delta = 5$ mm. Then, the experimental values of E_5 and $E_{BCN,6}$, which are given in the Table 3 and plotted in Figure 9a, were processed using the statistical application XLSTAT ©, obtaining the linear relationship of equation (6).

$$E_5(E_{BCN,6}) = 117.35 + 0.205 \cdot E_{BCN,6} \quad (6)$$

This equation fits very well the experimental results with a coefficient of determination (r^2) of 0.9628 and absolute differences lower than 1.7%, as can be also seen in Table 3.

As proposed in section 4, a correlation between E_{25} and $E_{BCN,6}$ was also obtained using XLSTAT ©. Eq. (7) shows this linear correlation which produced a r^2 of 0.9990.

$$E_{25}\left(E_{BCN,6}\right) = 63.55 + 3.479 \cdot E_{BCN,6} \quad (7)$$

Table 3 and Figure 9a show the results with this correlation. The very good correlation obtained confirms that establishing the correlation between E_{25} and $E_{BCN,6}$ is feasible and, in fact, better than using Eq. (6).

Table 3. Fit of equations (6), (7) and (8) to experimental data.

	exp.	exp.	$E_5(E_{BCN,6})$		exp.	$E_{25}(E_{BCN,6})$ linear		$E_{25}(E_{BCN,6})$ nonlinear	
Concrete	$E_{BCN,6}$ (J)	E_5 (J)	Eq. (6) (J)	Diff. (%)	E_{25} (J)	Eq. (7) (J)	Diff. (%)	Eq. (8) (J)	Diff. (%)
FRS–4	212	162	161	1.17	804	800	0.40	799	-0.52
FRS–6	290	174	177	-2.99	1065	1073	-0.77	1074	0.87
FRS–12	340	189	187	1.83	1252	1247	0.40	1247	-0.42

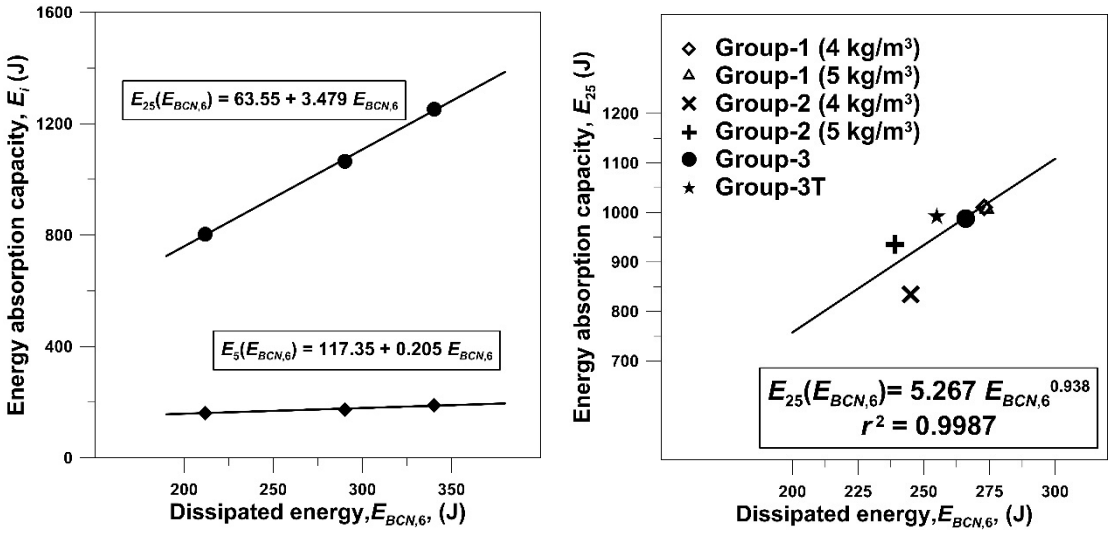

(a) (b)

Figure 9. (a) Comparison of linear correlation given by Eq. (6) and Eq. (7) with experimental data; (b) Comparison of Eq. (8) with results of the validation tests.

Nevertheless, with the aim to propose a code-type correlation for controlling the energy absorption capacity of shotcrete at works by means of BCN test, a nonlinear relationship of the form $y = a\,x^b$ between E_{25} and $E_{BCN,6}$ has been studied. In this equation a, and b, are experimental parameters which depend on the type of fibers used to reinforce the

concrete. These parameters have been determined using a nonlinear regression analysis by means of XLSTAT ©, obtaining the following equation:

$$E_{25}(E_{BCN,6}) = 5.267 \cdot (E_{BCN,6})^{0.938} \quad (8)$$

As can be also seen in Table 3 and Figure 9b, this equation fits very well the experimental data with a $r^2 = 0.9987$.

7. VALIDATION OF THE CORRELATION BETWEEN E_{25} AND $E_{BCN,6}$

To replace the panel test by the BCN test in the FRS control in the construction of mining tunnels in Chile, Eq. (8) was validated using the results obtained with two groups of samples of FRS prepared by a construction company that executed a section of the Chuquicamata Underground (*Chuquicamata Subterránea*) Project of CODELCO–Chile. The FRSs sampled were dosed to reach a compressive strength $f_c = 25$ MPa at 28 days, a slump of 24 cm, and reinforced with 4 kg/m^3 and 5 kg/m^3 of the same synthetic fibers BC – 54 used in laboratory research (Table 2). The concretes were mixed at industrial level and moved to the sprayed front point in mixer trucks and sprayed by mean of robots, as can be seen in Figure 1.

The FRSs were sampled by filling wood molds during the shotcrete spraying in the construction of the tunnel's support. After 48 hrs, the molds were transferred to an on-site laboratory, where cylindrical controls of 153 mm in diameter and variable length and panels with nominal dimensions of 600 × 600 × 100 mm were cut. It is worth noting that the panels were cut through their six faces using a water-cooled diamond saw. Subsequently, the specimens were transferred to the Laboratory of the Federico Santa María Technical University, where they were tested following the UNE 83515 standard and EFNARC recommendation. Prior to the tests, the controls were cut at a ratio of $H/d \approx 1$.

The results obtained in the BCN and panel tests of each series are presented in Table 4, in which are also presented the nominal amount of reinforcing fiber used in each studied shotcrete and the value of the energy absorption capacity estimated for each series using Eq. (8).

Table 4. Results of samples obtained at Chuquicamata Underground Project's works.

Group	Fiber amount (kg/m^3)	$E_{BCN,6}$ (J)	E_{25} (J)	Eq. (8) (J)	Difference (%)
1	4	273 (9.3)	1011 (5.0)	1016	0.45
	5	274 (15.6)	1007 (13.6)	1019	1.19
2	4	245 (13.4)	835 (19.2)	917	9.88
	5	239 (12.7)	936 (16.2)	896	-4.23

As can be observed in Table 4, the energy absorption capacity of the FRS estimated using Eq. (8) fits well with the experimental results obtained with the on-site samples, with a maximum difference of 9.88%, which can be graphically observed in Figure 9b. On the other hand, it is observed that the scatter of the results of the panel tests is higher than the difference in the dissipated energy results obtained with the BCN test, which ratifies one of the advantages of this test, and has been widely highlighted by different authors (Molins *et al*., 2009; Carmona *et al*., 2012; Cavalaro and Aguado, 2015).

8. APPLICATION OF THE PROPOSED CORRELATION

Considering the good fitting of Eq. (8), in the construction of the tunnels support in the Underground Chuquicamata Project, the use of the BCN test was proposed to verify the energy absorption capacity of the FRS already used in the linings. The dose of this FRS was (in kg/m^3): type IP cement = 450; gravel (5/10) = 81; sand (0/5) = 1533; water = 215; high range water reducing and superplasticizing admixture = 3.9; and plasticizer

admixture = 3.15. The average slump measured at work was 24.5 cm, and average compressive strength at 28 days f_c = 39.9 MPa.

For that purpose, the following procedure was used:

- Identify 15 points where panels were sampled and whose intra-sample absorbed energy values have a CoV lower than 20%.
- Drill at least 2 cores of 150 mm diameter from the shotcrete of the tunnel support at each of the selected points.
- Obtain the dissipated energy at $TCOD = 6.0$ mm of each core by means of BCN test.

Following the proposed procedure, the panel sampling points given in Table 5 were selected, along with the values of the energy absorption capacity obtained during the control.

Table 5. Energy absorption capacity and dissipated energy used to validate Eq. (8).

Sample	Sample point	Square panel tests				BCN tests			
		P – 1 (J)	P – 2 (J)	$E_{25,i}$ (J)	CoV (%)	T – 1 (J)	T – 2 (J)	$E_{BCN,6i}$ (J)	CoV (%)
1	7994.77 – 7997.96	978	1028	1003	3.5	276	292	284	4.0
2	68.382 – 73.170	1005	967	986	2.7	218	237	228	5.9
3	681.441 – 671.841	1036	1025	1031	0.8	**231**	**349**	**290**	**28.8**
4	22.66	986	979	983	0.5	292	258	275	8.7
5	20	1009	998	1004	0.8	305	305	305	0.0
6	85	996	977	987	1.4	244	208	226	11.3
7	40	990	986	988	0.3	**172**	**300**	**236**	**38.4**
8	124	1023	910	967	8.3	236	200	218	11.7
9	141.196 – 148.801	1000	1001	1001	0.1	230	220	225	3.1
10	50.91 – 53.427	940	1004	972	4.7	191	219	205	9.7
11	208.44 – 212.23	1020	1004	1012	1.1	287	295	291	1.9
12	50	1025	1014	1020	0.8	**254**	**177**	**216**	**25.3**
13	937	948	931	940	1.3	322	311	317	2.5
14	645.745	923	903	913	1.6	-	-	-	-

15	6809.221	932	904	918	2.2	-	-	-	-

At the same sampling points showed in Table 5, two cores of diameter d = 153 mm were drilled for the BCN test. Before tests, the cores were sawed to obtain a ratio $H/d \approx 1$. The tests were performed following the specifications and configuration given in standard UNE 83515 (Figure 4a) obtaining the results for each sample, also given in Table 5.

As can be seen in Table 5, two samples (number 14 and 15) were discarded because they failed suddenly when cracking load was reached, due to low fiber content. At the same time, the CoV of four samples, displayed in bold, are higher than 20% and, then, these results were also discarded.

With the mean values of dissipated energy, $E_{BCN,6}$ = 257 J the energy absorption capacity of shotcrete was determined by using of Eq. (8), obtaining $E_{25}(E_{BCN,6})$ = 961 J, which is plotted in Figure 9b as Group 3. This value differs -2.55% with respect to mean experimental value of E_{25} = 986 J.

On the other hand, using all the samples given in Table 8, an average value of dissipated energy $E_{BCN,6}$ = 255 J is reached. Then, replacing this value in the Eq. (8), the energy absorption capacity estimated is $E_{25}(E_{BCN,6})$ = 952 J, which is plotted as Group-3T in Figure 9b. This value differs by -3.97% with respect to the average E_{25} = 992 J obtained from the panel tests.

8.1. About the use of 100 mm diameter specimens

Because some shotcrete's thickness of the tunnel's linings of the Chuquicamata Underground Project are less than 150 mm, it was proposed to evaluate the properties of the FRS by means of the BCN test executed on 100 mm diameter cores. For this, a correction factor was developed to use Eq. (8) to determine the energy absorption capacity of the FRS.

Considering that a cylinder subjected to double punch loading fails normally with three cracks (Molins *et al*., 2009), the relationship between the theoretical cracking areas of both specimens is 2.25. This factor remains constant for different cracking observed at final state of the cylinders after being subjected to DPT, as shown in Figure 4b, it can be established the following expression:

$$E_{25}\left(E_{BCN,6-100}\right) = 5.257 \cdot \left(2.25 \cdot E_{BCN,6-100}\right)^{0.938} \quad (9)$$

Where $E_{BCN,6-100}$ is the dissipated energy by a 100 mm diameter cylinder at $TCOD$ = 6 mm.

To verify this relationship, an experimental campaign was carried out in which 14 square panels, sampled at seven different points when FRS was sprayed in the tunnels, were tested. This concrete reached a compressive strength f_c = 40.5 MPa at 28 days and was reinforced with 5 kg/m^3 of synthetic fibers BC–54, obtaining the results shown in Table 6.

Table 6. Testing results used to validate Eq. (9).

Sample	Panel	E_{25i} (J)	E_{25} (J)	$E_{BCN,6-100i}$ (J)	$E_{BCN,6-100}$ (J)
1	1a	849	817	82.5	91.0
	1b	785		99.5	
2	2a	783	784	62.0	67.7
	2b	785		73.4	
3	3a	761	806	84.2	87.2
	3b	851		90.2	
4	4a	884	847	83.0	91.0
	4b	809		99.0	
5	5a	790	813	107.7	104.8
	5a	835		101.8	
6	6a	717	709	82.6	102.8
	6b	701		123.0	
7	7a	969	843	103.43	91.5

	7b	717		79.52	

Using the results of Table 6, an average energy absorption capacity E_{25} =803 J with a CoV = 5.8% was obtained. From these panels, 100 mm diameter cores were cut, which were tested following the procedure given in standard UNE 83515, obtaining an average value of the dissipated energy $E_{BCN,6-100}$ = 90.85 J with a CoV = 13.4%. Replacing this value in Eq. (9), $E_{25}\left(E_{BCN,6-100}\right) = 803$ J was determined, which differs by 3.86% from the value of the average energy absorption capacity of the FRS determined before.

9. CONCLUSIONS

An equivalence between cracked square panel and cylinder under DPT was established based on the crack opening and, using this equivalence, a linear correlation was developed between energy absorption capacity determined by testing square panels and dissipated energy obtained with BCN test.

An experimental type-code relationship was developed between the EFNARC panel test and the double-punch Barcelona of a synthetic-fiber reinforced concrete to be used for controlling the FRS used in tunnel linings.

Furthermore, it is justified that a correlation between tests based on relating the fracture mechanisms is difficult due to the complexity of the failure mechanisms involved in the EFNARC panel; for light reinforcements, the fracture is predominantly caused by bending, whereas for significant reinforcements, the fracture is predominantly caused by punching.

The developed expression, as based on the testing of samples made in the laboratory with different amounts of reinforcing fiber, directly relates the energies of both tests without requiring other variables, such as the amount of fiber or the concrete's compressive strength, at least in the range of strengths analyzed.

The application of such a correlation to a concrete sprayed on-site using the same fiber has proven satisfactory, with a difference between the experimental and the correlated measurement of 2.6%. Therefore, it is possible to claim that the criterion and methodology used can be applied to other cases.

The benefit of using much smaller specimens that can be extracted from the actual lining is going to simplify and improve the quality control of the tunnels' support projects in addition to reducing the construction cost and the residue of such task.

10. APPENDIX – 1 INTERPRETATION OF THE PANEL RESULTS BASED ON THE BENDING RESULTS

10.1. Ultimate load of a slab knowing the fiber reinforced concrete bending strength

In case the panel breaks under bending, it should develop plastic failure mechanism and, knowing the sectional response of the concrete with fibers, it would be possible to calculate the maximum fracture load P for such a panel. The plastic analysis of the slab allows determining the plastic failure mechanism and the maximum load assuming that the moment-curvature diagram is perfectly plastic after cracking. In the $P - CMOD$ diagrams of the bending tests complementarily developed in the first laboratory investigation (see Figure 10), it was found that the idealization of a perfectly plastic behavior is fairly acceptable.

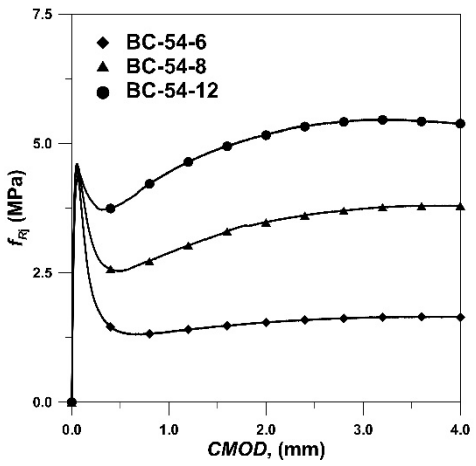

Figure 10. Average $P - CMOD$ curves obtained with the FRC tested.

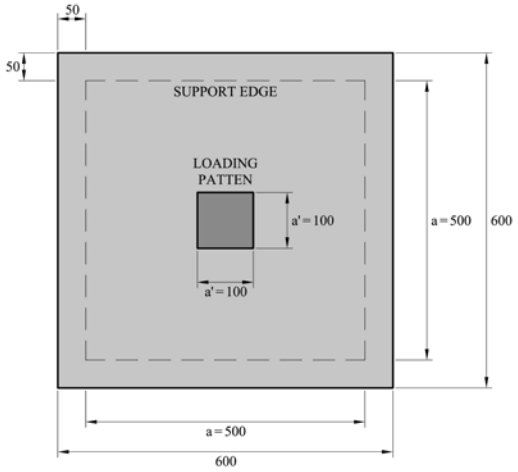

Figure 11. Geometry of the EFNARC panel with its perimeter support and loading plate.

A square slab subjected to a point load in its center, of a material whose bending response is isotropic and remains constant in all directions, develops a collapsing mechanism with four cracks, which start at the center, reach the midpoint of each side and divide the plate into four new square slabs (Figure 7a). On the other hand, it is not exactly a point load but is applied through a square steel plate with sides of 100 mm such that an approximately uniform load is applied. In this case, there is a direct expression that allows calculating the fracture load of a square plate with a centered squared uniform load, as is shown in Figure 11.

The analytical expression (Jimenez *et al.*, 2000) is shown in equation (4), where *m* is the plastic bending moment, a is the side of the slab, a' is the side of the loading plate, and *F* is the maximum load.

$$F = 24\, m \left(\frac{2a - a'}{a} \right)^{-2} \tag{10}$$

Applying this expression to a square slab with sides of 500 mm and a centered squared loading area with sides of 100 mm, the following ultimate load is obtained as a function of the resistant plastic moment:

$$F = 7.407\ m \tag{11}$$

Even though the span between the supports is exactly 500 mm, the hinges extend to the edge of the slab. To consider this additional bending capacity, the ratio between the length of the plate's side and that of the support's side is applied, as shown in Eq. (12).

$$F = 7.407\ m\ 6/5 \tag{12}$$

10.2 Obtaining the plastic bending moment per unit of length

To calculate the plastic bending moment, the average maximum residual strength of the 3PB tests on notched beams is adopted. From such residual strength, calculated according to the EN-14651 standard (CEN, 2005b), the Model Code 2010 (CEB – FIP, 2010) expression has been adopted for obtaining the residual strength according to Eq. (13).

$$f_{Tu} = 0.333F_{R3} \tag{13}$$

Once the post-cracking FRS tensile capacity is known, it is possible to calculate the plastic moment per unit of length assuming that the depth of the neutral axis under simple bending is negligible (Eq. 14).

$$m = f_{Tu}h^2/2 \tag{14}$$

Where h is the depth of the slab.

10.3 Effect of friction in the supports

During the panel test, sliding friction is produced in the supports (Bjøntegaard, 2009). When the panel rotates to descend under the load's pressure, it tends to separate the initial support lines. Given that the support frame is horizontally rigid, it is necessary for the horizontal force to overcome the friction force for movement to take place. The friction force can be calculated from the friction coefficient (μ) between the panel's concrete and

the steel of the support frame upon knowing the vertical force. According to Rabbat and Russell (1985), a coefficient of 0.57 has been adopted. Considering that relieving arches are formed in the two perpendicular directions of the panel's plane and that the supports are on the four sides of the frame, it is straightforward to assume that the normal load on each side is a fourth of the total.

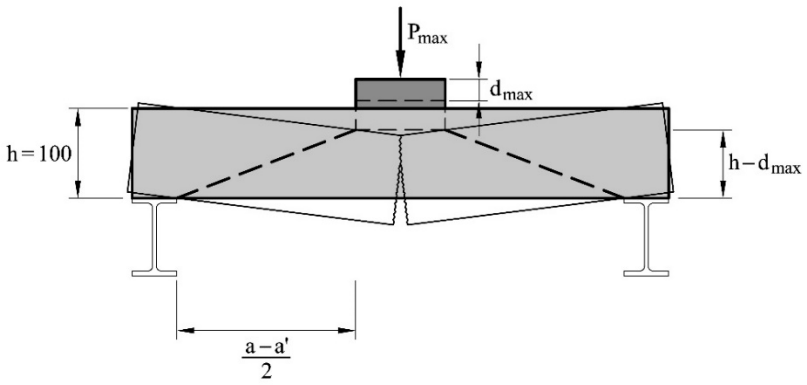

Figure 12. Geometry for the calculation of arch effect in the cracked panel.

On the other hand, it should be considered that the relieving arch rise is limited to the depth of the panel. However, for significant loads, the panel is already cracked, with a significant deflection that reduces the useful depth where the arch can be inscribed. Therefore, it will be necessary to consider the deflection at the center of the panel when calculating the panel's strength capacity through the arch effect (Figure 12).

Finally, the total additional load resisted by the panel through the arches in the two orthogonal directions can be estimated as:

$$F_{ARCH} = 2\ (\mu(P_{EFN} + W_{panel+platten)}/4)\frac{h - d_{max}}{(a - a')/2} \quad (15)$$

where F_{ARCH} is the force of the arch effect, P_{EFN} is the applied peak vertical load on the panel, $W_{panel+plate}$ is the panel's own weight plus the weight of the steel plate that transmits the load onto the concrete, h is the depth of the panel, a is the span between supports, a'

is the side of the loading plate, and d_{max} is the deflection corresponding to the peak experimental load P_{EFN}.

The resisted vertical load (P_{MAX}) can then be estimated as the sum of that resisted by bending of the slab and that resisted by the arch effect introduced by the friction force with the frame (equation 16).

$$P_{MAX} = F + F_{ARCH} \quad (16)$$

The results of the loads (P_{MAX}) estimated by equation (16) are compared with the experimental ones in Table 7. For the panel with 4 kg/m^3 of reinforcement, the estimated load (P_{MAX}) is similar to experimental one (11% less). However, for the panels with 8 and 12 kg/m^3, the estimated loads are significantly larger, 46% and 62%, respectively. The difference with the results of the EFNARC panel increases with increasing FRS bending capacity. That clearly shows that there is another mechanism that determines the failure, which is the FRS punching capacity.

Table 7. Estimated and experimental maximum loads, P_{MAX} and P_{EFN}, of the FRS panels.

FRS	F_{Rj} (MPa)	f_{Rj} (MPa)	m (Nmm/mm)	F (kN)	P_{EFN} (kN)	d_{max} (mm)	F_{ARCH} (kN)	P_{MAX} (kN)
FRS-4	2.106	0.702	3510	33.70	**44.7**	6.92	6.06	**39.76**
FRS-8	5.258	1.753	8763	84.13	**63.4**	7.60	8.48	**92.61**
FRS-12	8.807	2.936	14678	140.91	**94.3**	11.58	12.01	**152.92**

11. ACKNOWLEDGMENTS

This research was supported by Fondecyt Project “Use of the Generalized Barcelona Test for Characterization and Quality Control of Fiber Reinforced Shotcretes in Underground Mining Works”, N°1150881.

The authors thank the help of Vicepresidencia of CODELCO- Chile, ACCIONA Agencia Chile, Astaldi Sucursal Chile, Lem Laboratory, and Claudio Parada of Barchip Chile.

12. REFERENCES

AENOR, (2010) "UNE 83515 – Hormigones con fibras. Determinación de la resistencia a fisuración, tenacidad y resistencia residual a tracción. Método Barcelona". AEN/CTN 83 – Hormigón, Madrid (in Spanish).

Aire, C., Carmona, S., Aguado. A., Molins, C., (2015) "Double-Punch Test of Fiber-Reinforced Concrete: Effect of Specimen Origin and Size," ACI Materials Journal, V. 112, No 2, pp 199–208, doi.org/10.14359/51687362.

ASTM (2018), "C595/C595M-18, Standard Specification for Blended Hydraulic Cements", ASTM International, West Conshohocken, PA. www.astm.org.

Barton, N., Lien, R., Lunde, J., (1974) "Engineering classification of rockmass for the design of tunnel support", Rock Mechanics, V. 6, No 4, pp. 189 – 236.

Barton N., Bandis S.C., (1990) "Review of predictive capabilities of JRC-JCS model in engineering practice", Proceedings of the International Symposium on Rock Joints, Loen, Norway, pp. 603–610.

Bjøntegaard, Ø., (2009) "Energy absorption capacity for fibre reinforced sprayed concrete. Effect of friction in round and square panel tests with continuous support (Series 4)", Technical Report 2534, Norwegian Public Roads Administration Directorate of Public Roads Technology Department, 60 pp.

Carmona, S., Aguado, A., Molins, C., (2012) "Generalization of then Barcelona test for the toughness control of FRC", Materials and Structures, V. 45, No 7, pp. 1053 – 1069. doi.org/10.1617/s11527-011-9816-8.

Carmona, S., Aguado, A., Molins, C., (2013) “Characterization of the Properties of Steel Fiber Reinforced Concrete by Means of the Generalized Barcelona Test,” Construction and Building Materials, V. 48, pp. 592–600. Doi.org/10.1016/j.conbuildmat.2013.07.060

Carmona, S., Molins, C., Aguado, A., Mora, F., (2016) “Distribution of Fibers in SFRC Segments for Tunnel Linings”, Tunnelling and Underground Space Technology, V. 51, pp 238–249. Doi.org/10.1016/j.tust.2015.10.040.

Carmona, S., (2017) “Proyecto Chuquicamata Subterránea – Determinación de la capacidad de absorción de energía de shotcrete reforzado con fibras mediante el ensayo Barcelona”, Universidad Técnica Federico Santa María, Valparaíso, Chile, 2017, pp. 38 (in Spanish).

Carmona, S., Molins, C., (2017) “Application of BCN test for controlling fiber reinforced shotcrete in tunnelling works in Chile”, IOP Conference Series: Materials Science and Engineering Volume 246, Issue 1, 16 October 2017, Article number 012010, 9th International Conference Fibre Concrete 2017; Prague; Czech Republic; 13 September 2017 through 16 September 2017.

Carmona, S., Molins, C., Aguado, A., (2018) “Correlation between bending test and Barcelona tests to determine FRC properties”, Construction and Building Materials Journal, V. 181, pp. 673–686. Doi.org/10.1016/j.conbuildmat.2018.05.253.

Carmona, S., Molins, C., (2019) “Use of BCN test for controlling tension capacity of fiber reinforced shotcrete in mining works”, Construction and Building Materials, V. 198, pp. 399–410. Doi.org/10.1016/j.conbuildmat.2018.11.229.

Cavalaro, S., and Aguado, A., (2015) “Intrinsic Scatter of FRC: An Alternative Philosophy to Estimate Characteristic Values,” Materials and Structures, V. 48, No. 11, pp. 3537–3555. Doi.org/10.1617/s11527-014-0420-6.

CEB-FIP (2010), “Model Code – First Complete Draft,” FIB Bull vol. 1, V. 55, pp. 1–318.

CEN (2005a), EN 14488–1 Testing sprayed concrete — Part 1: Sampling fresh and hardened concrete. 10 pp.

CEN (2005b) European Committee for Standardization, “EN 14651: Test Method for Metallic Fibered Concrete–Measuring the Flexural Tensile Strength (Limit of Proportionality (LOP), Residual)”, 17 pp.

CEN (2006), “EN 14488-5:2006 Testing sprayed concrete. Determination of energy absorption capacity of fibre reinforced slab specimens”, 8 pp.

Chao, S. H., Karki, N. B., Cho, J. S., Waweru, R. N. (2012), “Use of Double Punch Test to Evaluate the Mechanical Performance of Fiber Reinforced Concrete,” In Parra-Montesino, Reinhardt, Naaman, editors. Proceedings of the 6th International Workshop on High Performance Fiber Reinforced Concrete Composites (HPFRCC 6), Ann Arbor, Michigan, pp.27–34.

Choumanidis, D., Badogiannis, E., Nomikos, P., Sofianos, A. “Barcelona test for the evaluation of the mechanical properties of single and hybrid FRC, exposed to elevated temperature”, Construction and Building Materials, V.138, 2017, pp. 296–305. Doi.org/10.1016/j.conbuildmat.2017.01.115

Conforti, A., Minelli, F., Plizzari, G A., Tiberti, G., (2017) “Comparing test methods for mechanical characterization of fiber reinforced concrete”, Structural Concrete, pp. 1- 14. Doi.org/10.1002/suco.20170057.

EFNARC (1996), European Specification for Sprayed Concrete. European Federation of National Associations of Specialist Contractors and Material Suppliers for the Construction Industry, 30 pp.

Galeote, E., Blanco, A., Cavalaro, S. H. P. De la Fuente, A., “Correlation between the Barcelona test and the bending test in fibre reinforced concrete”, Construction and Building Materials, V. 152, 2017, pp. 529–538. Doi.org/10.1016/j.conbuildmat.2017.07.028

Geocontrol Andina, “Especificaciones Técnicas Detalladas; Trabajos en mina, Línea 2 y Ramal Av. Faucett–Av. Gambetta de la Red Básica del Metro de Lima y Callao,” Perú, 2015, 78 pp (in Spanish).

Kuehl, R. (2001), “Diseño de Experimentos: Principios Estadísticos para el Diseño y Análisis de Investigaciones”, Thomson Learning, 2ª edición, 666 pp (in Spanish).

Jiménez, P., García, A., Morán F., (2000) “Hormigón Armado”, Ed. Gustavo Gili, ISBN: 9788425218255, 846 pp. (in Spanish).

Kim, J., Lee, G. P., Moon, D. Y., (2015) “Evaluation of Mechanical Properties of Steel-Fibre-Reinforced Concrete Exposed to High Temperatures by Double-Punch Test,” Construction and Building Materials, V. 79, pp. 182–191. Doi.org/10.1016/j.conbuildmat.2015.01.042.

Molins, C., Aguado, A. and Mari, A., (2006), “Quality control test for SFRC to be used in precast segments”, Tunnelling and Underground Space Technology, V. 21, No 3, pp. 423-424. Doi.org/10.1016/j.tust.2005.12.067.

Molins C., Aguado A. and Saludes S., (2009), “Double Punch Test to Control the Energy Dissipation in Tension of FRC (Barcelona Test),” Material and Structures, V. 42, No 4, pp. 415–425. Doi.org/10.1617/s11527-008-9391-9.

Pros, A., Diez, P., Molins, C., “Numerical Modeling of the Double Punch Test for Plain Concrete,” International Journal of Solids and Structures, V. 48, 2011, pp. 1229–1238.

Pros, A., Diez, P., Molins, C., “Modeling Steel Fiber Reinforced Concrete: Numerical Immersed Boundary Approach and a Phenomenological Mesomodel for Concrete–Fiber

Interaction," International Journal for Numerical Methods in Engineering, V. 90, 2012, pp. 65–86.

Pujadas, P., Blanco, A., Cavalaro, S., De la Fuente, A., Aguado, A., "Analytical Model that Allows a Generalization of the Barcelona Test by Using the Axial Displacement to Determine the Toughness of the FRC," Journal of Civil Engineering and Management, V.19, No. 2, 2013, pp. 259–271. Doi.org/10.3846/13923730.2012.756425.

Pujadas, P., Blanco, A., Cavalaro, S.H.P., De la Fuente, A., Aguado, A., "Multidirectional double punch test to assess the post-cracking behavior and fibre orientation of FRC", Construction and Building Materials, V. 58, 2014, pp. 214–224. Doi.org/10.1016/j.conbuildmat.2014.02.

Rambo, D. A. S., Blanco, A., Figueiredo, A. D., Santos, E. R. F., Filho, R. D. T., Gomes, O. F. M., "Study of temperature effect on macro-synthetic fiber reinforced concretes by means of Barcelona tests: An approach focused on tunnels assessment", Construction and Building Materials, V. 158, 2018, pp. 443–453. Doi.org/10.1016/j.conbuildmat.2017.10.046

Rabbat, B. and Russell, H., (1985) "Friction Coefficient of Steel on Concrete or Grout2, J. Struct. Eng., V. 111, pp. 505-515.